Available online at www.sciencedirect.com
ScienceDirect
European Journal of Mechanics B/Fluids 26 (2007) 271–283

Scaling of the near-wall layer beneath turbulent separated flow

P.E. Hancock

Fluids Research Centre, School of Engineering, University of Surrey, Guildford, Surrey, GU2 7XH, UK

Received 1 August 2005; received in revised form 15 March 2006; accepted 9 May 2006

Available online 29 September 2006

Abstract

This paper is a continuation of an earlier paper [P.E. Hancock, Velocity scales in the near-wall layer beneath reattaching turbulent separated and boundary layer flows, Eur. J. Mech. B Fluids 24 (2005) 425–438] in which it is proposed that each Reynolds stress has its own velocity scale. Two of these, u'_τ and w'_τ, are directly related by definition to the r.m.s. of the wall-shear-stress fluctuations (τ_x and τ_z) in the streamwise and transverse directions. They are also velocity scales for the true dissipation of the turbulent kinetic energy and the Kolmogorov velocity and length scales at the surface. From asymptotic considerations it is shown that the other two scales are related to averages involving instantaneous gradients of wall-shear-stress fluctuations. The measurements, made using pulsed-wire anemometry into the viscous sublayer, show that u'_τ and w'_τ are also the velocity scales for the respective streamwise and transverse fourth-order velocity moments, together with the viscous velocity scale (ν/y). Normalised, the fourth-order moments show an inner-layer-like behaviour independent of both position *and* direction, like that seen in the second-order moments [P.E. Hancock, Velocity scales in the near-wall layer beneath reattaching turbulent separated and boundary layer flows, Eur. J. Mech. B Fluids 24 (2005) 425–438]. However, not surprisingly, the third order moments exhibit an effect of mean shear, seen in the skewing of the probability distributions. Though not measured directly, the measurements imply the behaviour of the averaged products of fluctuations in wall-shear-stress and wall-pressure-gradient ($\overline{\tau_x \partial p/\partial x}$ and $\overline{\tau_z \partial p/\partial z}$). Normalised, they also are independent of position and direction. Some of the results presented apply more generally to the near-wall region beneath turbulent flow.

Keywords: Turbulent separated flow; Near-wall layer

1. Introduction

In most circumstances of practical interest in wall-bounded turbulent flow it is necessary to model to at least some degree the flow immediately adjacent to surface. This is so, for example, for Large Eddy Simulation at high Reynolds number, where the current computational capability, though impressive, is still not sufficient to allow the near-wall region to be adequately resolved. Indeed, better modelling of the near-wall region is one of the pressing needs of LES as a method [1]. Very near the surface viscous effects dominate and the velocity is usually presumed to behave according to the classical viscous sublayer, except for fully resolved numerical simulations where no such assumption is required. At high Reynolds numbers a deeper region needs to be modelled.

E-mail address: p.hancock@surrey.ac.uk (P.E. Hancock).

0997-7546/$ – see front matter
doi:10.1016/j.euromechflu.2006.05.006

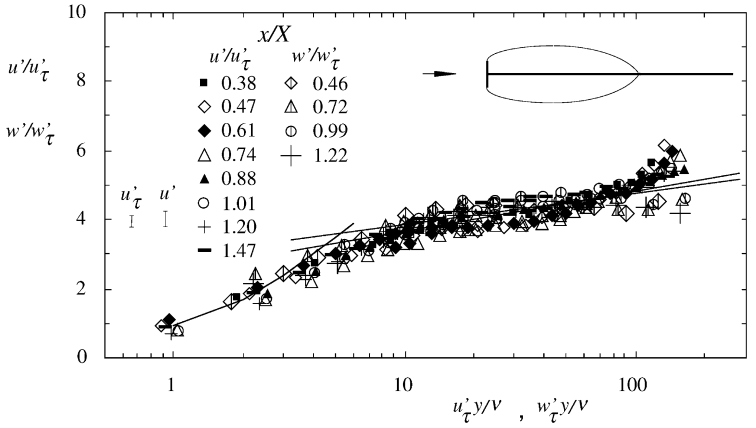

Fig. 1. u' and w' in wall units of Eqs. (1.1) and (1.2), from [3]. Vertical bars indicate error limits in u'_τ, w'_τ and u', w'. Inset figure illustrates flow rig and dividing streamlines (not to scale) $x/X = 0$ and 1 denote separation and reattachment positions.

The present paper stems from observations made both from the authors own measurements and those of Song et al. [2] (hereafter S) for the flow beneath separated and boundary layer flows, and is a sequel to an earlier paper (hereafter H). Pulsed-wire velocity and wall shear stress measurements beneath a separated flow, reported in H, showed that the r.m.s of the streamwise and lateral fluctuations, u' and w' scale according to

$$\frac{u'}{u'_\tau} = f_u\left(\frac{u'_\tau y}{\nu}\right) \quad \text{and} \tag{1.1}$$

$$\frac{w'}{w'_\tau} = f_w\left(\frac{w'_\tau y}{\nu}\right) \tag{1.2}$$

in an 'inner layer', without any apparent influence of the mean velocity profile, where u'_τ and w'_τ are velocity scales based on the wall shear stress fluctuations in the streamwise and lateral directions (x and z), respectively. $u'_\tau = \sqrt{\tau'_x}$ where τ'_x is the r.m.s of the kinematic wall-shear-stress fluctuation, τ_x, in the x-direction, with a corresponding definition for w'_τ. y is the perpendicular distance from the surface and ν is the kinematic viscosity. Also, not only was it found that the functions f_u and f_w are identical, but that there appears to be a logarithmic region, beneath which there is a viscous and buffer layer, reminiscent of the mean velocity profile in the inner layer of a standard boundary layer. The existence of a logarithmic region can be argued in the familiarly classical way, but with application to the turbulence rather than mean flow, if the gradients in u' and w' depend only on u'_τ/y and w'_τ/y. Asymptotically, of course, as y becomes very small, $u'/u'_\tau = u'_\tau y/\nu$ and $w'/w'_\tau = w'_\tau y/\nu$ for any flow but, as will be observed here, there is no significant extent of a linear viscous sublayer. Fig. 1 is from H and shows u' and w' according to the above scaling, where these measurements were obtained beneath a two-dimensional turbulent separation bubble, formed downstream of a sharp-edged laminar separation, as illustrated in the inset of Fig. 1. It can be seen that u' and w' follow the form of Eqs. (1.1) and (1.2) out as far as $u'_\tau y/\nu \approx w'_\tau y/\nu \approx 70$, beyond which u'/u'_τ clearly rises above w'/w'_τ. Quantitatively the same behaviour as seen in Fig. 1 was found from the measurements of S, not only near reattachment but also near separation, which in their case was for a turbulent boundary layer separating from a smooth wall. It was argued that fluctuating flow reversals beneath a separating turbulent boundary layer are not unlike the fluctuating flow reversals near reattachment. The 'logarithmic-law' line having the larger slope in Fig. 1 is given by $u'/u'_\tau = 2.5 + 0.5\ln(u'_\tau y/\nu)$ and the sub-layer line,[1] details of which are given in [4], comes from assuming an oscillating viscous layer driven by a sinusoidally oscillating pressure gradient as described by the equation $\partial u/\partial t = \partial p/\partial x + \nu\partial^2 u/\partial y^2$, where p is the kinematic pressure.

Drawing on the measurements of both S and H, H went on to explore the idea that each Reynolds stress has its own velocity scale. In addition to the scales of u'_τ and w'_τ for, respectively, u' and w', the wall-normal r.m.s velocity v' and the Reynolds shear stress $\overline{uv}$ also have velocity scales, denoted v'_0 and s'_0, respectively, such that

[1] Inadvertently, this line was referred to in H as a quadratic layer because it is asymptotically quadratic. The author apologises for the confusion.

$$\frac{\upsilon'}{\upsilon'_0} = f_\upsilon\left(\frac{\upsilon'_0 y}{\nu}\right) \quad \text{and} \tag{1.3}$$

$$\frac{s'}{s'_0} = f_s\left(\frac{s'_0 y}{\nu}\right), \tag{1.4}$$

where $s = |\overline{uv}|^{1/2}$. Fig. 2 shows the variation of υ' and s' as measured by S in terms of Eqs. (1.3) and (1.4), where υ'_0 and s'_0 were chosen so as to give consistency with these forms, as described in H. Although, the scales do not have the immediate interpretation available to u'_τ and w'_τ they are in fact linked to u'_τ and w'_τ, as will be presented later.

A feature of the near-wall layer is that the mean velocity gradients are low compared with those in the outer part, except very near the surface where the flow is viscous-dominated and $\partial U/\partial y$ at the surface is about three orders of magnitude larger than it is further out. (Fig. 3 is an example.) In terms of turbulent kinetic energy production the production in the near-wall region is small and negative or negligible compared with that in the outer flow (Le et al. [5]). Fig. 1 and Eqs. (1.1) and (1.2) in effect represent predominantly the 'footprint' of the 'inactive' motion [6] of the outer flow.

One of the objectives in the present paper is to ask whether the apparent simplicity of the above equations and Fig. 1 apply in type to higher-order moments, as they would if the motion were 'universal', or whether for some reason such a scaling does not extend beyond second order. Another and related objective is to investigate the apparently negligible effect of the mean shear immediately adjacent to the surface. If the fluctuations above this region are, say, unskewed (in terms of their probability density function) then a positive-going mean motion could be anticipated to give rise to

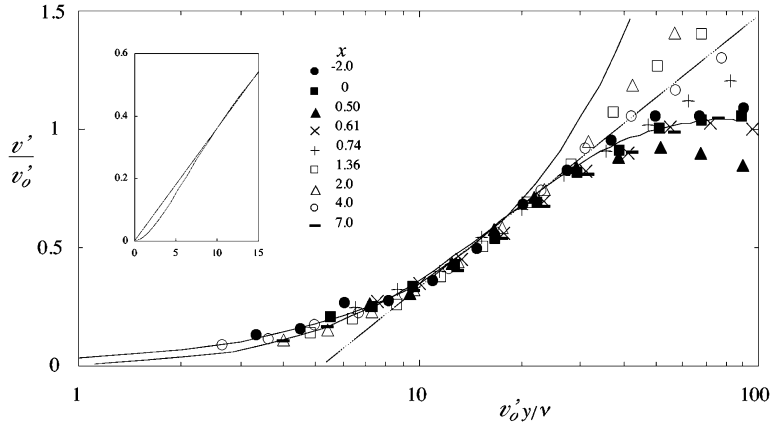

(a)

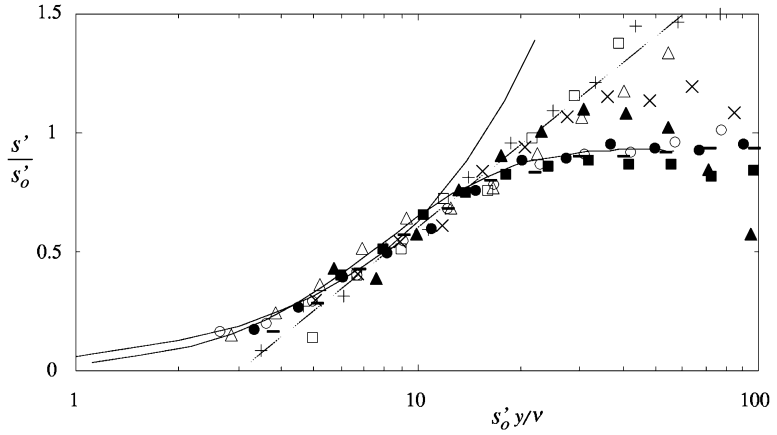

(b)

Fig. 2. (a) υ' and (b) s' in wall units of Eqs. (1.3) and (1.4). Full lines: linear relationship and Moser et al. [8]. Broken line from H.

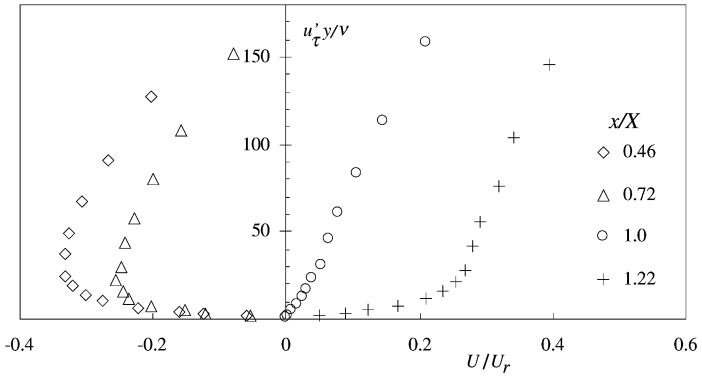

Fig. 3. Mean velocity profiles at $x/X = 0.46$, 0.72, 1.0 and 1.22.

positive skewness in the fluctuations very near the surface and in the surface shear stress [7], with the converse in the reverse-flow region. Also, asymptotic considerations were only briefly made in H – they are considered in detail here.

2. Asymptotic considerations

2.1. Wall-parallel velocities

If, in the usual way, very near the surface the inertial forces can be neglected then the *instantaneous* streamwise and lateral velocity fluctuations are given by

$$u = \frac{\tau_x}{\nu} y + \frac{1}{\nu}\frac{\partial p}{\partial x} y^2 + \frac{b_u}{\nu} y^3 + \cdots, \tag{2.1}$$

$$w = \frac{\tau_z}{\nu} y + \frac{1}{\nu}\frac{\partial p}{\partial z} y^2 + \frac{b_w}{\nu} y^3 + \cdots, \tag{2.2}$$

where, here, τ_x, τ_z, $\partial p/\partial x$ and $\partial p/\partial z$ are instantaneous kinematic shear stress and pressure gradient fluctuations at the wall, and b_u, b_w are the coefficients of the third terms. (In that these equations are linear in velocity, wall shear stress and pressure, equations of the same form apply to the mean + plus + fluctuating counter-parts, and therefore apply to the mean and fluctuating parts separately. Only the latter need be considered here.) Production of turbulent kinetic energy, if it is significant, is expected to vary as y^3 and so it anticipated that it is at least legitimate to consider terms to order y^2, though the expansions are considered to higher order in some places on the basis that the production appears to be small or negligible. From Eq. (2.1) the r.m.s of u, denoted by u', is of the form

$$u' \approx \frac{y}{\nu}\left[\overline{\tau_x^2} + \overline{\frac{\partial p}{\partial x}\tau_x}\, y + \left(\frac{1}{4}\overline{\left(\frac{\partial p}{\partial x}\right)^2} + 2\overline{b_u \tau_x}\right) y^2 + \cdots\right]^{1/2},$$

where the overbar denotes the time-average. At sufficiently small y

$$u' = \frac{y u_\tau'^2}{\nu}\left[1 + \frac{1}{2}\frac{1}{u_\tau'^4}\overline{\frac{\partial p}{\partial x}\tau_x}\, y + \frac{1}{2}\frac{1}{u_\tau'^4}\left(\frac{1}{4}\overline{\left(\frac{\partial p}{\partial x}\right)^2} + 2\overline{b_u \tau_x}\right) y^2 + \cdots\right],$$

i.e.

$$\frac{u'}{u'_\tau} \approx \frac{y u'_\tau}{\nu} + \frac{1}{2}\frac{\nu}{u_\tau'^5}\overline{\frac{\partial p}{\partial x}\tau_x}\left(\frac{y u'_\tau}{\nu}\right)^2 + \frac{1}{2}\frac{\nu^2}{u_\tau'^6}\left(\frac{1}{4}\overline{\left(\frac{\partial p}{\partial x}\right)^2} + 2\overline{b_u \tau_x}\right)\left(\frac{y u'_\tau}{\nu}\right)^3 + \cdots. \tag{2.3}$$

Similar expressions follow for w' by rotation of terms. Asymptotically, the sub-layer line shown in Fig. 1 is of the form

$$\frac{u'}{u'_\tau} = \frac{y u'_\tau}{\nu} - a\left(\frac{y u'_\tau}{\nu}\right)^2, \tag{2.4}$$

where a is about 0.1. Thus, we see that $\overline{(\partial p/\partial x)\tau_x}$ and likewise $\overline{(\partial p/\partial z)\tau_z}$ must be negative, and when normalised with $u_\tau'^5/\nu$ and $w_\tau'^5/\nu$, respectively, are about -0.2. On average, a positive wall shear stress fluctuation is associated with an instantaneously negative pressure gradient, irrespective of the mean flow direction in the case of u and in the absence of a mean flow in the case of w.

In passing it is worth noting that the mean square of the pressure gradient, part of the third term in Eq. (2.3), is necessarily positive. Were this part significant and the other part negligible then there would be an increase in u' with y^3 in Fig. 1, contrary to what is observed. Thus, the effect of the mean square of the pressure gradient appears to be small unless the other part counter-balances it. The absence of any sizeable effect is consistent with the pressure field being determined primarily by the large-scale outer-flow structures – i.e. with the pressure controlled primarily by inactive motion.

2.2. Dissipation, viscous diffusion and pressure terms

If $\varepsilon_{u0}, \varepsilon_{w0}$ and $\varepsilon_{\upsilon 0}$ are the contributions to the (true) kinematic dissipation of turbulent kinetic energy, $\varepsilon = \overline{\nu(\partial u_i/\partial x_j + \partial u_j/\partial x_i)^2}$, in the respective transport equations for $\overline{u^2}$, $\overline{w^2}$ and $\overline{\upsilon^2}$ then it is straightforward to show that, at $y = 0$,

$$\varepsilon_{u0} = \frac{1}{\nu} u_\tau'^4, \tag{2.5}$$

$$\varepsilon_{w0} = \frac{1}{\nu} w_\tau'^4, \tag{2.6}$$

$$\varepsilon_{\upsilon 0} = 0, \tag{2.7}$$

where the suffix zero denotes the surface, and where υ is the wall-normal velocity (equations for υ are discussed below). Thus, u_τ' and w_τ' are also scales of the respective contributions to the dissipation at the surface, ε_0, given by

$$\varepsilon_0 = \frac{1}{\nu}\left(u_\tau'^4 + w_\tau'^4\right). \tag{2.8}$$

Consequently, the Kolmogorov velocity and length scales $((\nu\varepsilon)^{1/4}$ and $(\nu^3\varepsilon)^{1/4})$ at the surface are given straightforwardly by, respectively, $(u_\tau'^4 + w_\tau'^4)^{1/4}$ and $\nu(u_\tau'^4 + w_\tau'^4)^{-1/4}$. These expressions and Eqs. (2.5)–(2.8) are true at the surface for any flow.

Near $y = 0$

$$\varepsilon_u = \frac{u_\tau'^4}{\mu}\left[1 + 2\frac{1}{u_\tau'^4}\overline{\frac{\partial p}{\partial x}\tau_x}\, y + \mathrm{O}\left(y^2\right) + \cdots\right]$$

i.e.

$$\varepsilon_u = \frac{u_\tau'^4}{\mu}\left[1 + 2\frac{\nu}{u_\tau'^5}\overline{\frac{\partial p}{\partial x}\tau_x}\frac{u_\tau' y}{\nu} + \mathrm{O}\left(y^2\right) + \cdots\right] \tag{2.9}$$

with a similar equation for ε_w, and $\varepsilon_\upsilon = \mathrm{O}(y^2)$. As it happens, the term $(\nu/u_\tau'^5)\overline{(\partial p/\partial x)\tau_x}$ also appears in Eq. (2.3) and was noted as being negative, implying an initially linear decrease in dissipation as y increases from zero. Although u' increases with y, the decrease in dissipation is presumably because the instantaneous gradients of u are decreasing with increasing distance from the surface.

2.3. Wall-normal velocity

From Eqs. (2.1) and (2.2) it follows that

$$\upsilon = -\frac{1}{\nu}\left\{A\frac{y^2}{2} + B\frac{y^3}{6} + C\frac{y^4}{4} + \mathrm{O}\left(y^5\right)\right\},$$

where

$$A = \frac{\partial \tau_x}{\partial x} + \frac{\partial \tau_z}{\partial z}, \quad B = \frac{\partial^2 p}{\partial x^2} + \frac{\partial^2 p}{\partial z^2} \quad \text{and} \quad C = \frac{\partial b_u}{\partial x} + \frac{\partial b_w}{\partial z}$$

leading to

$$\upsilon' = \frac{y^2}{\nu}\left\{\frac{\overline{A^2}}{4} + \frac{\overline{AB}}{6}y + \left(\frac{\overline{AC}}{4} + \frac{\overline{B^2}}{6}\right)y^2 + \cdots\right\}^{1/2}, \tag{2.10}$$

where as usual the leading term shows the r.m.s. velocity, υ', to vary with y^2, with y^3 the next most significant term. Similarly, the leading term for $\overline{uv}$ is y^3 followed by y^4.

Taking the leading term in Eq. (2.10) it follows that for small y

$$\frac{\upsilon'}{\upsilon'_0} = \left(\frac{\upsilon'_0 y}{\nu}\right)^2 \frac{\nu}{\upsilon_0'^3}\overline{\left(\frac{\partial \tau_x}{\partial x} + \frac{\partial \tau_z}{\partial z}\right)^2}^{1/2}.$$

If this represents a behaviour consistent with Eq. (1.3) then the latter part of the right hand side must be constant, leading to

$$\upsilon_0'^3 \propto \nu\overline{\left(\frac{\partial \tau_x}{\partial x} + \frac{\partial \tau_z}{\partial z}\right)^2}^{1/2}.$$

The same process leads to

$$s_0'^5 \propto \nu\overline{\tau_x\left(\frac{\partial \tau_x}{\partial x} + \frac{\partial \tau_z}{\partial z}\right)}.$$

These equations show that υ'_0 and s'_0 are related to spatial *gradients* of the wall shear stress fluctuation, which is to be expected in that υ is related to $\partial u/\partial x$ and $\partial w/\partial z$.

Figs. 2(a) and 2(b) show the variation of υ' and s' and as measured by S in terms of Eqs. (1.3) and (1.4), where the profiles of υ' fall impressively close to a single curve to about as far as $\upsilon'_0 y/\nu = 30$, the impressiveness underlining the quality of their measurements. Concurrence between the profiles of s' is somewhat less – but then the scatter within a profile is generally larger – extending about as far as $s'_0 y/\nu = 15$. (Closer agreement requires changes of s'_0 of only 1% or less.) In these measurements, which were made above a curved backward-facing step, –2 corresponds to the upstream zero-pressure-gradient turbulent boundary layer. The smooth-wall separation was at about 0.77 and reattachment at about 1.36. For further details see S and H where, as described in the latter, it was shown that υ'_0 and s'_0 could be chosen so as to collapse the measurements on to those of the zero-pressure gradient boundary layer (for which υ'_0 and s'_0 were arbitrarily taken as equal to the mean friction velocity). The figures also show (i) the DNS data of Moser et al. [8] normalised in the same way as the experimental data, (ii) a linear variation between υ' and y, and (iii) the 'log-law' lines given in H.

As can be seen from Fig. 2(a), the variation of υ' with y is closely linear rather than as y^2, with $\upsilon'/\upsilon'_0 = 0.035\upsilon'_0 y/\nu$ giving a good fit to the measurements out as far as about $\upsilon'_0 y/\nu = 15$. This of course is an inviscid behaviour, and is not covered by the asymptotic analysis earlier. Very near $y = 0$ υ' must very as y^2 as illustrated in the inset diagram, taken from the data of Moser et al. Their computations indicate that viscous effects extend to about $\upsilon'_0 y/\nu = 8$ and, albeit rather tentatively, the trend of the measurements falls closer to the viscous line below this height. Although s' is more scattered these data are closer to a linear variation, with $s'/s'_0 \approx 0.063 s'_0 y/\nu$ – but only out as far as $s'_0 y/\nu \approx 8$ – than they are to either $y^{3/2}$ (viscid) or $y^{1/2}$ (inviscid), making the behaviour of s' a 'mixture' of inviscid and viscid.

3. Experimental techniques

The experimental set up is described in H, as are details concerning configuration and accuracy of the pulsed-wire and wall shear stress probes and the associated techniques, and so will not be repeated here in full. Very briefly, the separation bubble was downstream of a sharp-edged normal flat plate, of tip-to-tip height 23.8 mm, mounted on a thin horizontal splitter plate, supported on the centre line of the working section of height 500 mm. A simplified sketch of the plates is shown in the inset of Fig. 1. The upstream free stream speed, U_r, was 5.9 m/s, the bubble length, X, was 216 mm, and the flow width 7.1 bubble lengths [9].

As discussed in H the pulsed-wire velocity probe gives a systematic error in regions of high velocity gradient, giving errors in the measured mean and fluctuating velocities near a surface. A method of correction is given by Hancock [4] but was applied only to the mean and r.m.s. of the fluctuation by use of correction factors (of the ratio

'true'/'measured'). The method of correcting the mean velocity is iterative, using consistency with the mean wall shear stress as measured by the pulsed-wire wall shear stress probe (which does not suffer the same error) as a condition. The correction factor for the r.m.s. is then obtained explicitly, where concurrence with the expected behaviour in the viscous-dominated region very near the surface and the measured r.m.s. wall-shear-stress fluctuation gives confidence in the accuracy of the correction. The errors were significant only beneath $u'_\tau y/\nu$, $w'_\tau y/\nu$ of 10 and sometimes significant only below 3. The reader is referred to [4] for further detail on the errors.

The method assumes a sinusoidally imposed oscillation in the flow above an idealised viscous sublayer. This means that the same approach cannot be used when it comes to correcting $\overline{u^3}$ or the skewness S_u, because the 'true' $\overline{u^3}$ is always zero. However, the method can be used to give a guide as to the size of the error generated, by calculating the departure from zero of the (predicted) measured skewness, $\overline{u_m^3}/(\overline{u_m^2})^{3/2}$. The magnitude of this quantity exceeded 0.1 only beneath $u'_\tau y/\nu$ of 10, and sometimes only beneath 2. At reattachment it was essentially zero. Its largest value was 0.48 at $u'_\tau y/\nu$ of 1 (at $x/X = 0.74$ and 1.2 – see later). So, $\overline{u^3}$ and S_u are taken to be unaffected by this gradient error above $u'_\tau y/\nu = 10$ in general, and a lower height in some instances.

With the fourth order moment the same sort of correction procedure can be employed as for $\overline{u^2}$, namely to calculate a correction factor $\overline{u^4}/\overline{u_m^4}$. It turns out that the factor $(\overline{u^4}/\overline{u_m^4})^{1/4}$ is very close to the factor for the r.m.s., u'/u'_m $(= (\overline{u^2}/\overline{u_m^2})^{1/2})$ given in [4] (Fig. 8), to within between 0 and 3% discrepancy.

$\overline{w^4}$ was not measured because it requires in principle the probe to be oriented at five or more different angles such that the inversion matrix is non-singular, more than the minimum number being the usual practice in pulsed-wire anemometry in order to provide a self-consistency check and reduce errors. However, as measurements were in any case made with both the velocity and shear stress probes oriented at angles $\pm 45^\circ$ to the streamwise direction, making the probes sensitive to $(u \pm w)/\sqrt{2}$ and $(\tau_x \pm \tau_z)/\sqrt{2}$, respectively, some inferences can be drawn regarding $\overline{w^4}$ from the fourth-order moments of velocity and the r.m.s. of the shear-stress fluctuations obtained at these angles.

The only other point that need be mentioned here is that pulsed-wire anemometry has a 'blind spot' – a velocity or a wall shear stress level below which the probe cannot measure, depending on the construction of the probe, the pulse strength and the sensitivity of the sensor wires. Here, the width of the velocity blind spot was about ± 0.3 m/s, and negligible for the shear stress. Samples within the blind spot are taken as zero, and so appear as a spike in a probability distribution function (pdf). It turns out that the error in velocity or shear stress moments is negligible provided the zeros are included, a point that was reconfirmed in the course of earlier work [10]. The gradient error discussed above affects the pdf distribution with the effect of widening it, for the few points nearest the wall. These and the associated histograms have been corrected by adjusting the mean to concur with the corrected mean (as given by [4]) and adjusting the fluctuation magnitude by the correction factor used for u'. This preserves the shape – i.e. the skewness – of the pdf and gives the correct $\overline{u^4}$ to within the error limit discussed earlier.

4. Results and discussion

Measurements were made at four positions along the bubble: $x/X = 0.46$, 0.72, 1.0 and 1.22. The mean velocity profiles are shown in Fig. 3, where the gradient arising directly from the viscous constraint $U = 0$ is predominant beneath about $u'_\tau y/\nu \approx 20$. The lateral mean velocity, W, which should be zero, was smaller than $0.01U_r$.

The third-order moment, $\overline{u^3}$, is shown in Fig. 4, normalised by u'^3_τ, as a function of $u'_\tau y/\nu$, for the four stations. The departure of any point from its profile is much less than the variation between profiles, the departure being comparable with the expected error band for this quantity of about ± 5. Evidently, the profiles do not demonstrate any universality inside, say, $u'_\tau y/\nu = 70$, though the variation between profiles is least near $y = 0$. At and downstream of reattachment $\overline{u^3}/u'^3_\tau$ levels off as y increases, whereas at the two stations upstream it rises. Fig. 5 shows the skewness factor in both linear and semi-logarithmic axes. These figures also give the skewness factor from the wall shear stress probe, shown at $u'_\tau y/\nu = 1$, and Fig. 5(b) shows trend lines ignoring some of the velocity measurements closest to the surface, for reasons given in Section 3.

Profiles of forth-order moments, $\overline{u^4}$, are shown in Fig. 6(a), normalised by u'^4_τ, as a function of $u'_\tau y/\nu$, while Fig. 6(b) shows the same data but in terms of $\overline{u^4}^{1/4}/u'_\tau$ as a function of $u'_\tau y/\nu$. Fig. 7 shows $\overline{u^4}^{1/4}/u'_\tau$, again as a function of $u'_\tau y/\nu$, but in semi-logarithmic axes, Fig. 7(a) showing the uncorrected measurements and Fig. 7(b) the corrected measurements, as discussed in Section 3 (and which have been presented in Fig. 6). The concurrence

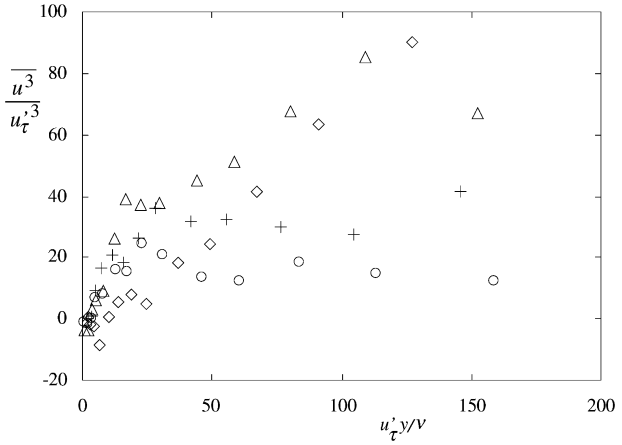

Fig. 4. $\overline{u^3}$ normalised by u'_τ. Symbols as in Fig. 3.

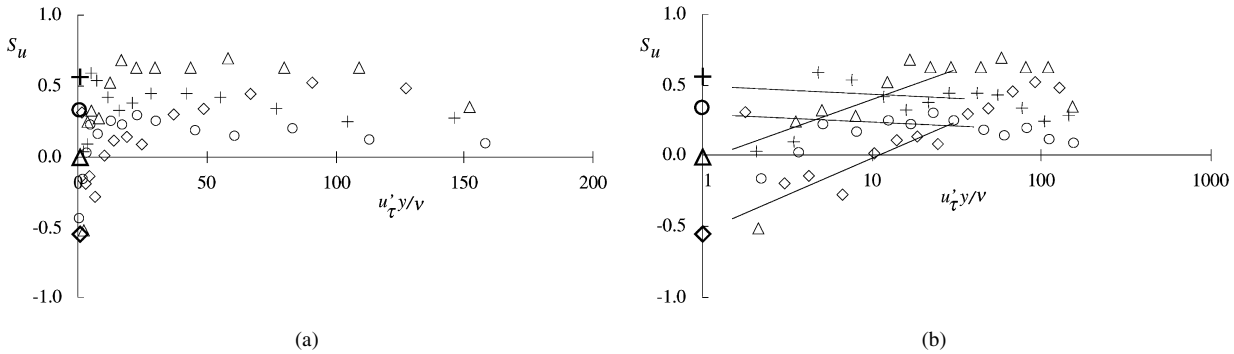

Fig. 5. Skewness factor, S_u, in (a) linear axes, (b) semi-logarithmic axes. Symbols as in Fig. 3. Larger symbols at $u'_\tau y/\nu = 1$ are skewness factors from wall shear stress probe.

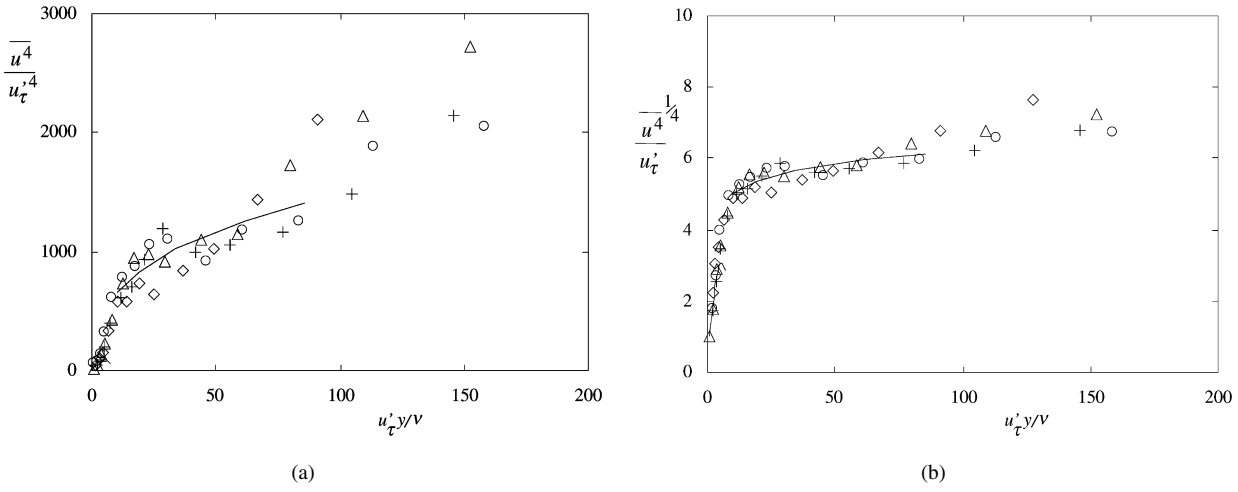

Fig. 6. Forth-order moment of u (a) $\overline{u^4}$, (b) $\overline{u^4}^{1/4}$. Symbols as in Fig. 3.

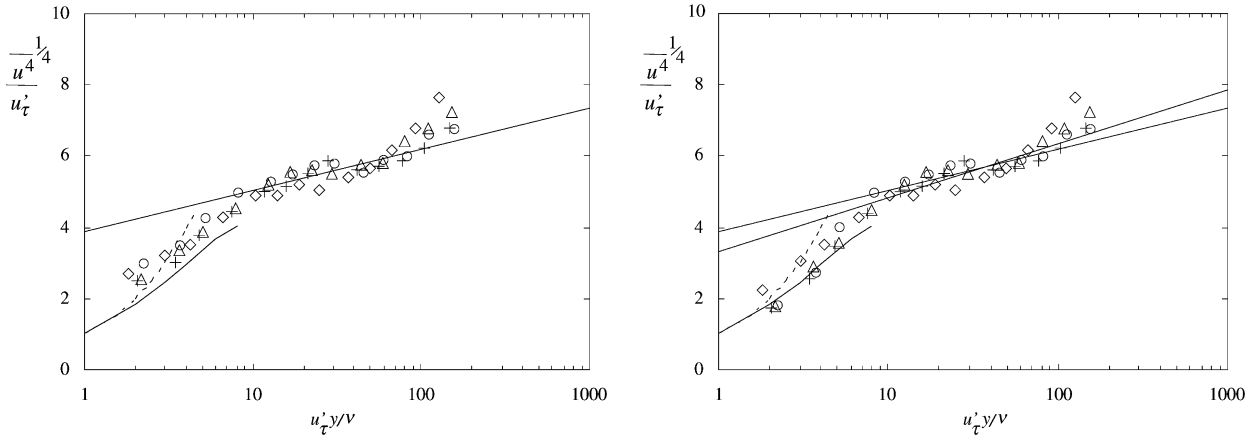

Fig. 7. $\overline{u^4}^{1/4}$ in semi-log axes (a) before correction, (b) after correction. Symbols as in Fig. 3. Broken line is linear sublayer. Other lines – see text.

between the four profiles is remarkably close, particularly as the fourth moment by definition draws heavily on the fluctuations at the edges of the pdf, demonstrating that,

$$\frac{(\overline{u^4})^{1/4}}{u'_\tau} = g\left(\frac{u'_\tau y}{\nu}\right),$$

over a substantial streamwise fetch beneath the bubble. The latter figure, Fig. 7(b), shows close concurrence with a viscous sublayer and, between $u'_\tau y/\nu$ of about 10 and 70, with a plausibly logarithmic behaviour, which follows if $\mathrm{d}(\overline{u^4}^{1/4})/\mathrm{d}y$ scales on u'_τ/y. The logarithmic-law line shown in Fig. 7(b) having the lower slope is given by

$$\frac{(\overline{u^4})^{1/4}}{u'_\tau} = 3.9 + 0.5\ln\left(\frac{u'_\tau y}{\nu}\right),$$

which is also shown in Fig. 6. As will be seen below, the flatness factor is constant at about 3.2, above $u'_\tau y/\nu \approx 10$. The steeper 'log-line' in Fig. 7(b) is from the original fit to u' in Fig. 1, giving an intercept and slope of 3.3 and 0.66 (i.e. $2.5 \times 3.2^{1/4}$ and $0.5 \times 3.2^{1/4}$), respectively, in Fig. 7(b). Similarly, the 'log-line' of lower slope in Fig. 1 is from the lower-slope line in Fig. 7(b), giving an intercept and slope of 2.96 and 0.39, respectively. Arguably, there is not a great deal to choose between the two lines, which in any case can be regarded as empirical fits.

Beneath $u'_\tau y/\nu \approx 8$ the measurements generally agree well for three of the four profiles with a non-linear sub-layer form based on the analysis given in [4]. Straightforward extension of that analysis leads to $\overline{u^4} = 1.5\overline{u^2}^2$, or that $\overline{u^4}^{1/4} = 1.107u'$.[2] The sublayer curve shown in Fig. 7 is, to second order given by $(\overline{u^4})^{1/4}/u'_\tau = 1.107\{u'_\tau y/\nu - 0.09(u'_\tau y/\nu)^2\}$ beneath $u'_\tau y/\nu \approx 3$, emphasising as for u' the significant non-linearity of the sub-layer. Inferences could be drawn following that in Section 2, such as that $\overline{\tau_x^3 \partial p/\partial x}$ at the wall must also be negative, but this is not pursued further here. Of course, $\overline{\tau_x^4}^{1/8}$ could be proposed as a velocity scale for $\overline{u^4}$, instead of that supposed here, namely $\overline{\tau_x^2}^{1/4}$, but as can be seen from Fig. 8, the flatness of the wall shear stress fluctuations is constant to within the uncertainty in the measurements.

The flatness factor of the velocity fluctuations is shown in Fig. 9 in linear and semi-logarithmic axes, where the flatness from the wall shear stress measurements is also shown, at $u'_\tau y/\nu = 1$. There is a clear rising trend from the level of about 3.2 at and above $u'_\tau y/\nu \approx 10$, to about 5 at the wall.

Fig. 10 shows $\overline{u^4}^{1/4}/u'_\tau$ as a function of $u'_\tau y/\nu$, where u and u'_τ are temporarily defined to be in a direction of either $\pm 45°$. As outlined in Section 3, this provides an indication of the behaviour of $\overline{w^4}^{1/4}$. Fig. 10 also repeats data

[2] Independent of the parameter $\delta_0 u'_\tau/\nu$ in [4].

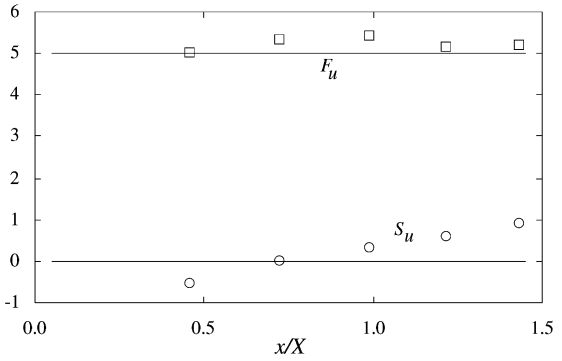

Fig. 8. Flatness and skewness factors of wall shear stress fluctuations.

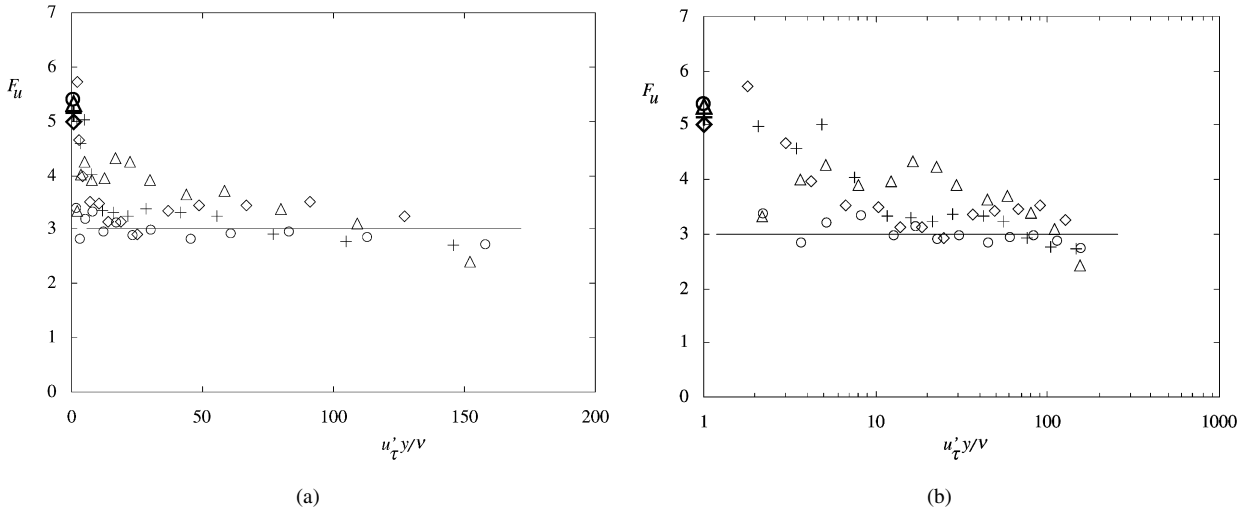

Fig. 9. Flatness factor, F_u; (a) in linear axes, (b) semi-logarithmic axes. Larger symbols at $u'_\tau y/\nu = 1$ in (a) and (b) are flatness factors from wall shear stress probe.

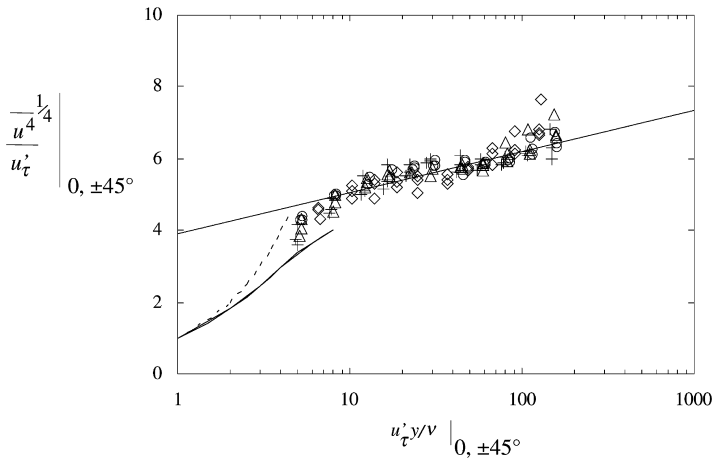

Fig. 10. $\overline{u^4}^{1/4}/u'_\tau$ with probes aligned at 0 and $\pm45°$. See text. Symbols as in Fig 3. Other lines as in Fig. 7(a).

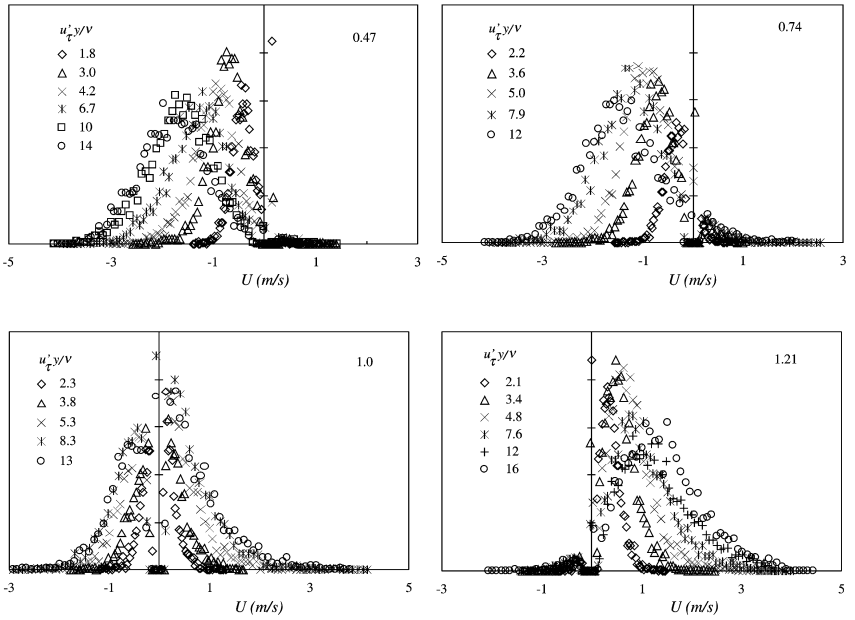

Fig. 11. Histograms of velocity fluctuations. U is absolute velocity.

given in Fig. 7(b); the inference drawn here is that $\overline{w^4}^{1/4}/w'_\tau$ as a function of $w'_\tau y/\nu$ behaves in exactly the same way as $\overline{u^4}^{1/4}/u'_\tau$ depends on $u'_\tau y/\nu$.

Histogram data is shown in Fig. 11 and pdf data in Fig. 12 for each of the four stations, with profiles grouped in the latter according to where $u'_\tau y/\nu$ is less than ~ 14, between ~ 14 and ~ 60, and above ~ 60. The pdf, $p(u)$, is normalised by u' so that area under each profile, $\int u' p(u)\,\mathrm{d}(u/u')$, is unity. The first group is where the mean velocity changes rapidly (see Fig. 3), as indeed can be seen by the shift in the centre of the profiles in Fig. 11. The second group is in the 'log law' region of Fig. 1 and where the mean velocity is also approximately constant, and the third group includes those beyond $u'_\tau y/\nu$ of 70. All the histograms are plotted to the same scale; in a few instances the spike at zero velocity is too large to be shown. Each point in the two figures was obtained from 3000 samples taken (slowly) over 300 seconds. The velocity has been corrected for the effect of gradient error by the approximation described in Section 3, for those measurements nearest the surface. This may mean there is still some error due to gradient effects in the other profiles near zero velocity, though instantaneously steep gradients further from the wall are supposed to be much less frequent than is the case immediately adjacent to the surface.

The bottom row of Fig. 12 shows profiles (at the larger $u'_\tau y/\nu$) that are all broadly similar in shape, slightly asymmetric, with a steeper side on the negative velocity side and more excursions to a higher positive velocity. The mean velocity, however, changes sign between the left two, where it is negative, and the right two, where it is positive (Fig. 3). These higher positive excursions are associated with the flow further out still (outer-layer structures). In contrast, the top row of Fig. 12 shows profiles (at the smallest $u'_\tau y/\nu$) where a distinct change in asymmetry can be seen between that at 1.22, where the profiles are much like those further out, and that at 0.46, where the mean velocity is negative. So, near the surface, there is an association between the sign of asymmetry with the sign of the mean velocity. The inference is that, at 0.46, this is the influence of the flow at an *intermediate* distance (from inner-layer structures) where the mean velocity is still negative. This influence from the flow at an intermediate distance also occurs at the later stations but because the mean velocity is positive it is 'reinforced' rather than 'opposed' by the influence of the flow at still greater distance, and so not seen. Therefore, the lack of similarity in the pdfs is simply a consequence of the flow near the surface depending on the flow structures in its immediate vicinity and on those further out – i.e. on both inner-layer and outer layer structures. In fact it would be rather odd if the pdfs exhibited similarity, and hence that the skewness factor, S_u, was constant. The skewness factors, S_u, already discussed are of course a quantification of the asymmetry of the pdf profiles, but the above discussion is more easily made by reference to the pdfs rather than just S_u. The pdfs in the middle row of Fig. 12 exhibit shapes that are intermediate between those of the top and bottom rows. Depending on how the skewed shape of the pdf changes, u'_τ may not strictly be a

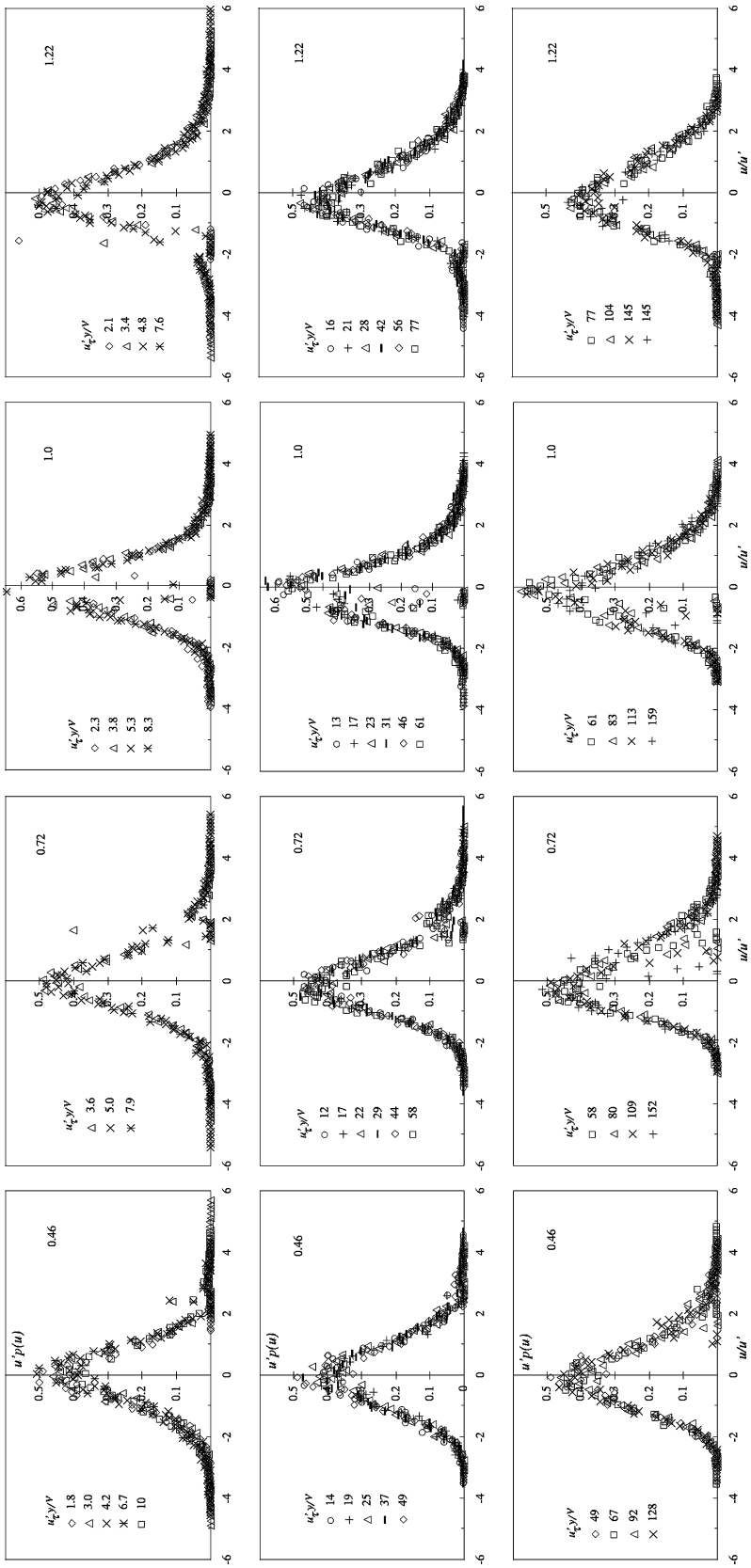

Fig. 12. Probability density function, $u'p(u)$ at various $u'_\tau y/\nu$ and x/X.

scale for $\overline{u^4}$ as well as for $\overline{u^2}$. Supposing a skewed pdf (with both sides Gaussian in shape but unequal in extent) shows that a Skewness factor of either ± 0.5 leads to a Flatness factor larger by only 5%, and therefore an inconsistency in $\overline{u^4}^{1/4}/u'_\tau$ of only 1%. This discrepancy is well within the uncertainty of the present measurements. In conclusion, the fact that $\overline{u^3}$ does not scale on u'_τ, while $\overline{u^2}$ and $\overline{u^4}$ do, does not invalidate the idea or use of u'_τ as a velocity scale.

Finally, as noted in Section 2, $(\nu/u'^5_\tau)\overline{(\partial p/\partial x)\tau_x}$, and its lateral counterpart, is about -0.2. If indeed this quantity is constant it follows that the wall shear stress fluctuations are determined solely by the pressure fluctuations at the surface, wherever they originate from in the flow above. This could explain why in H it was observed that, beneath $u'_\tau y/\nu \approx 3$, $u'/u'_\tau \sim u'_\tau y/\nu$ appears to behave in the same way for both the present flow and for a standard zero-pressure-gradient boundary layer, where there is a peak in u'/u'_τ in the near-wall layer at $u'_\tau y/\nu \approx 10$, this peak perhaps behaving as an outer-layer at very small distances.

5. Concluding remarks

The measurements show that u'_τ is also a suitable scale for the forth-order moment, $\overline{u^4}$, beneath $u'_\tau y/\nu \approx 70$; beneath this limit, $\overline{u^4}^{1/4}/u'_\tau$ is function only of $u'_\tau y/\nu$, at least over the distance $0.46 < x/X < 1.22$. What is more, $\overline{u^4}^{1/4}/u'_\tau$ plausibly follows a logarithmic and buffer-sublayer region. By inference, w'_τ, is also the relevant scale for $\overline{w^4}$, with $\overline{w^4}^{1/4}/w'_\tau$ exhibiting the same functional dependence on $w'_\tau y/\nu$ as does $\overline{u^4}^{1/4}/u'_\tau$ on $u'_\tau y/\nu$. Thus, in this framework, the near-wall turbulence is axisymmetric.

The not surprising finding that $\overline{u^3}$ does not scale on u'_τ does not invalidate u'_τ as a scale, but does mean there is an effect of mean shear strain on the turbulence structure, seen here in the skewing of *p(u)*, most evident immediately adjacent to the surface. Although for the present flow $\overline{w^3}$ is (ideally) zero, it is anticipated the same sort of effect will be seen in $\overline{w^3}$ beneath a three-dimensional separated flow, where $\overline{w^3}$ will in general not be zero [11].

As well as being scales for the respective tangential velocity fluctuations, u'_τ and w'_τ are also scales of the near-wall dissipation and the Kolmogorov velocity scale. The conventional friction velocity gives the mean-flow dissipation in expressions analogous to Eqs. (2.8) and (2.9). Rather nicely, the measurements can be used to infer that the products $\overline{(\partial p/\partial x)\tau_x}$ and $\overline{(\partial p/\partial z)\tau_z}$ are about $-0.2u'^5_\tau/\nu$ and $-0.2w'^5_\tau/\nu$, respectively. Both these products would be hard to measure accurately in a direct way, requiring simultaneous measurement of instantaneous wall shear stress and instantaneous pressure gradient.

The velocity scales v'_0 and s'_0, identified in H from the measurements of S, are related to instantaneous gradients in the wall shear stress but, though they are phenomenologically related to u'_τ and w'_τ, they cannot be expressed in terms of them. v'_0 and s'_0, were obtained indirectly; direct measurement would be an interesting challenge. v'/v'_0 behaves inviscidly above $v'_0 y/\nu \approx 8$ and in accord with Eq. (1.3) out to about $v'_0 y/\nu = 30$. The behaviour of s' is less clear.

Acknowledgements

As also noted in the earlier paper, the author is particularly grateful to Dr. Simon Song for making his measurements available in electronic form.

References

[1] U. Piomelli, E. Balaras, Wall-layer models for large-eddy simulations, Annu. Rev. Fluid Mech. (2002) 349–374.
[2] S. Song, D.B. DeGraaff, J.K. Eaton, Experimental study of a separating, reattaching, and redeveloping flow over a smoothly contoured ramp, Int. J. Heat Fluid Flow 21 (2000) 512–519.
[3] P.E. Hancock, Velocity scales in the near-wall layer beneath reattaching turbulent separated and boundary layer flows, Eur. J. Mech. B Fluids 24 (2005) 425–438.
[4] P.E. Hancock, Pulsed-wire measurements in the near-wall layer in a reattaching separated flow, Exp. Fluids 37 (2004) 323–330.
[5] H. Le, P. Moin, J. Kim, Direct numerical simulation of turbulent flow over a backward-facing step, J. Fluid. Mech. 330 (1997) 349–374.
[6] A.A. Townsend, The Structure of Turbulent Shear Flow, Cambridge University Press, 1976.
[7] P.E. Hancock, Measurements of mean and fluctuating wall shear stress beneath spanwise-invariant separation bubbles, Exp. Fluids 27 (1999) 53–59.
[8] R.D. Moser, J. Kim, N.N. Mansour, Direct numerical simulation of turbulent channel flow up to $Re = 590$, Phys. Fluids 11 (4) (1999) 943–945.
[9] F. Ciampoli, P.E. Hancock, Effects of flow width in nominally two-dimensional turbulent separated flows, Exp. Fluids 40 (2006) 196–202.
[10] P.E. Hancock, Low Reynolds number two-dimensional separated and reattaching turbulent shear flow, J. Fluid Mech. 410 (2000) 101–122.
[11] P.E. Hancock, Measurements of mean and fluctuating wall shear stress beneath spanwise-invariant separation bubbles, Exp. Fluids 27 (1999) 53–59.